Effect of Turbulence Layer Height and Satellite Altitude on Tropospheric Scintillation on Ka-band Earth-LEO Satellite Links

Weiwen Liu, and David G. Michelson, *Senior Member, IEEE*

***Abstract*—Tropospheric scintillation on Earth-space paths increases greatly at low elevation angles and/or higher carrier frequencies, may impair low margin systems and can interfere with power control algorithms used to mitigate rain fading. The amplitude and spectral characteristics of tropospheric scintillation have been well studied for Earth-GEO links which have fixed elevation angles and path lengths. However, little has been previously reported concerning tropospheric scintillation on Earth-LEO links which are distinguished by the rapid change of the elevation angle as the satellite passes from horizon to horizon. In such cases, both the length of the slant path to the turbulence layer and the velocity at which the slant path passes across the turbulence layer change rapidly as the satellite passes across the sky. This affects both the intensity of the scintillation process, which generally reaches its maximum value at low elevation angles and/or during periods of rain, and the corner frequency of the scintillation process, which generally reaches its maximum value at high elevation angles. Here we use a geometric model of propagation through the turbulence layer during a LEO satellite pass in conjunction with Tatarskii's theory of propagation through turbulent media to show that the corner frequency of the scintillation process increases: (i) as the orbital altitude decreases and (ii) as the height of the turbulence layer increases. We also discuss the implications of our results for simulation of tropospheric scintillation on Earth-LEO links**

***Index Terms*—fading channel, Ka-band, millimeter-wave radio propagation meteorological factor, satellite communications, scintillation.**

I. Introduction

In recent years, Ka-band Earth-space links have attracted considerable attention from service providers wishing to take advantage of the broader spectrum allocations (and less congestion), higher system bandwidths (and higher data rates), reduced interference potential and smaller equipment size (especially smaller antennas) compared to lower frequencies [1]. Although most existing Ka-band Earth-space links are used to increase the capacity of conventional communications satellites located in geostationary Earth orbit (GEO) [2], much recent interest has focused on the use of Ka-band links to provide high speed data communications with satellites in low Earth orbit (LEO) during the relatively short time that a satellite passes within range of an Earth station.

A decade ago, interest in Ka-band links to satellites in LEO was driven largely by the efforts of Iridium, Teledesic and others to develop large constellations of LEO satellites capable of providing voice services and/or broadband wireless access across the globe and the need to provide such constellations with high speed Earth-space access and/or feeder links [3]. Although commercial interest in the technology diminished for a time as confidence in the business models that supported the development of such networks diminished, interest in Ka-band links to LEO has experienced resurgence in recent years. High speed links based upon Ka-band technology are now seen as an increasingly viable method for reducing the cost of: (i) downloading gigabytes of data from scientific and Earth observation satellites during a single pass over an earth station, e.g., [4] and/or (ii) transferring terabytes of data between Earth stations at widely separated locations by using specialized LEO communications satellites or *datasats* to implement high capacity store-and-forward-based schemes, e.g., [5].

Although rain fading and tropospheric scintillation on Earth-space links are both more pronounced at Ka-band than at lower frequencies and can greatly affect link performance, very little channel measurement data has been collected on Ka-band Earth-LEO links. For various reasons, any plans that NASA or ESA might have had to conduct measurement programs aimed at characterizing fading on Ka-band Earth-LEO links following completion of the successful Earth-to-geostationary-orbit (Earth-GEO) Ka-band measurement programs of the 1990's (Olympus, ACTS, ITALSAT) never materialized. Although Iridium LLC and Teledesic have both collected at least some Ka-band propagation data, none of this data has been published or referred to in the open literature. Sample data from several FedSat passes over Australia were reported in 2005 [6], but

Manuscript received January 14, 2009, revised November 23, 2009, accepted 29 December 2009. This work was supported in part by grants from MacDonald Dettwiler and Associates, Western Economic Diversification Canada, and the Natural Sciences and Engineering Research Council of Canada.

W. Liu is with the University of British Columbia, Department of Electrical and Computer Engineering, Vancouver, BC V6T 1Z4 Canada. (e-mail: weiwenl@ece.ubc.ca).

D. G. Michelson is with the University of British Columbia, Department of Electrical and Computer Engineering, Vancouver, BC V6T 1Z4 Canada. (phone: 604-822-3544; fax 604 822-5949; e-mail: davem@ece.ubc.ca).

little else has been released to date. As a result, measurement-based channel models for Ka-band LEO links do not yet exist.

Without a better understanding of the Ka-band Earth-LEO channel, it is difficult for designers to set link budgets and/or design and implement appropriate fade mitigation techniques. Until more extensive measurement programs are undertaken, simulation based upon reasonable models of the atmosphere is likely the best option for developing useful insights. Moreover, such an approach also provides a basis for evaluating and interpreting measurement data sets once they become more generally available. In [7], we used simulations based upon realistic synthetic rain field models to show how the rapid motion of a LEO satellite across the sky leads to steeper fade slopes than in the well-studied case of links to geostationary satellites, *e.g.,* [8],[9]. In this paper, we focus on the scintillation that is the result of the signal passing through layers of atmospheric turbulence and/or rain.

Experience has shown that tropospheric scintillation increases greatly at low elevation angles and/or higher frequencies, may impair low margin systems and can interfere with power control algorithms used to mitigate rain fading. Current understanding of the physics of tropospheric scintillation is largely based upon the theoretical treatment developed by Tatarskii [10] in the early 1960's. It is based upon earlier work by Kolmogorov that predicts both the lognormal distribution of signal amplitude over the short term and the characteristic form of the corresponding power spectrum. A summary is presented in an appendix to this paper.

During the past twenty years, many researchers have conducted measurement-based studies of the amplitude and spectral characteristics of scintillation on Earth-GEO links, which are distinguished by their fixed elevation angles and path lengths. During the course of these studies, researchers have determined how the parameters of the scintillation process depend upon the height and thickness of the turbulence layer, the elevation angle of the slant path, tropospheric refractivity and water vapour content, wind speed, rain rate, carrier frequency and the size of the antenna aperture, and observed the manner in which the parameters of the scintillation process vary diurnally, seasonally and with geographic location [11]-[22].

With the exception of unpublished work such as [23], little has been reported concerning scintillation on Earth-LEO links. On such links, the satellite passes from horizon to horizon over several minutes and the motion of the satellite across the sky causes rapid changes in both the length of the slant path to the turbulence layer and the velocity at which the slant path passes across the turbulence layer. In this work, we use a geometric model of propagation through the turbulence layer during a LEO satellite pass in conjunction with Tatarskii's theory in order to obtain plausible estimates of: (i) the evolution of the scintillation process over Ka-band Earth-LEO links during a pass and (ii) how scintillation will be affected by the altitude of the satellite and the height of the turbulence layer. The results will permit more effective assessment of the performance of scintillation suppression techniques and the effect of scintillation on fade mitigation techniques.

The remainder of this paper is organized as follows: In Section II, we summarize current understanding of the turbulent layers that lead to scintillation. In Section III, we show how the parameters of the scintillation process can be estimated given knowledge of the look angle and angular velocity of the satellite across the sky and the height of the turbulence layer. In Section IV, we show how the motion and look angle of the satellite affects both: (i) the amplitude of the scintillation process, which generally increases as the elevation angle decreases and/or rain rate increases, and (ii) the corner frequency of the scintillation process, which generally increases as the elevation angle increases and the height of the turbulence layer increases. In Section V, we propose a method for generating scintillation time series that evolve in the appropriate manner during course of a pass so that our results may be more readily applied in system simulations. Finally, in Section VI, we summarize our findings and offer recommendations for future work.

II. Characterization Of Turbulence on Earth-Space Paths

Scintillation is randomly occurring constructive and destructive interference caused by rapid, random fluctuations of the atmospheric refractive index caused by turbulent mixing of air masses with different temperatures and water vapour content. As an incident wave is randomly refracted by the turbulence, different versions of the incoming signal will arrive at the receiving antenna from different directions and with different amplitudes and phases. On Earth-GEO links, scintillation occurs as turbulence cells are advected past the propagation path by the wind. Analysis of scintillation events observed on such paths has long suggested that the turbulence that gives rise to the phenomenon resides in a relatively thin layer at the top of the planetary boundary layer, a relatively moist layer of air ranging from the surface of the earth up to a few kilometers [11].

Recent work has considerably refined our understanding of the turbulent layers that give rise to scintillation. In particular, it has been shown that the turbulent layers responsible for scintillation on slant paths are typically located at the topside of clouds, particularly fair weather cumulus clouds, where they are the result of an air entrainment mechanism. Measurement data collected over Belgium during a twelve-month period using a radiosonde suggests that in mid-latitude climates: (i) the layer height falls between 500 and 5000 metres and is well characterized by a Rician distribution and (ii) the layer thickness is well characterized by a lognormal distribution with a median value of about 100 metres. Unlike the layer height and thickness, both the layer occurrence and the intensity of the turbulence were found to exhibit seasonal variability [12].

The essential aspects of the Tatarskii-Kolmokorov theory of propagation through random media and demonstration that its assumptions apply to Ka-band Earth-space paths are presented in the Appendix. The refractive index structure constant C_n^2 is a widely used measure of atmospheric turbulence. It ranges in

value from 10^{-10} $m^{-2/3}$ for a highly turbulent atmosphere to 10^{-20} $m^{-2/3}$ for weak turbulence [16]. Because the locus that defines the intersection of the slant path and the turbulence layer covers a broad extent during a typical LEO satellite pass, knowledge of the horizontal distribution of C_n^2 is essential for the simulation of scintillation on Earth-LEO links. Research concerning the horizontal distribution of atmospheric turbulence is still in its earliest stages, however, and much remains to be learned [24].

Previous measurements of scintillation on Earth-GEO links suggests that C_n^2 will be relatively constant over periods of at least to ten or fifteen minutes [16]. If one assumes that the turbulence cells are advected by wind at a velocity of 10 m/s, this duration corresponds to a horizontal extent of between 6 and 9 km. However, for layer heights ranging from 1 to 5 km and elevation angles above 10 degree, the locus that defines the intersection of the slant path and the turbulence layer may extend for between 10 and 50 km. While this implies that it might not be reasonable to assume that the structure constant is uniform over the entire field, we make that assumption here for lack of a better alternative.

III. Prediction of Scintillation Parameters on Earth-LEO Paths

A. Look Angle and Range Determination for LEO Satellites

The position of a satellite during a pass is defined by its azimuth, elevation and range relative to the earth station. The great circle (or Riemannian circle) angle γ between the earth station and the sub-satellite point can be determined by constructing the spherical triangle shown in Fig. 1 and applying the law of cosines to yield

$$\gamma = \arccos\left(\sin(L_s)\sin(L_e)+\cos(L_s)\cos(L_e)\cos(l_s-l_e)\right), \quad (1)$$

where L_e and l_e are the latitude and longitude of the earth station, respectively and L_s and l_s are the latitude and longitude of the subsatellite point, respectively. The azimuth angle of the subsatellite point S relative to the earth station can be determined by applying the law of sines to yield the interior angle

$$\phi_{\text{int}} = \arcsin\left(\frac{\cos L_s}{\sin\gamma}\sin|l_s-l_e|\right), \quad (2)$$

then accounting for the quadrant in which the subsatellite point is located relative to the earth station. The sublayer point P falls on the geodesic that links the Earth station E and the subsatellite point S.

A cross-section of the great circle that contains the earth station E, the sub-satellite point S, and the sub-layer point P is shown in Fig. 2. Applying the law of sines yields an expression for the elevation angle θ

$$\theta = \arcsin\left(\frac{R_E+H}{d}\sin\gamma\right)-\frac{\pi}{2}, \quad (3)$$

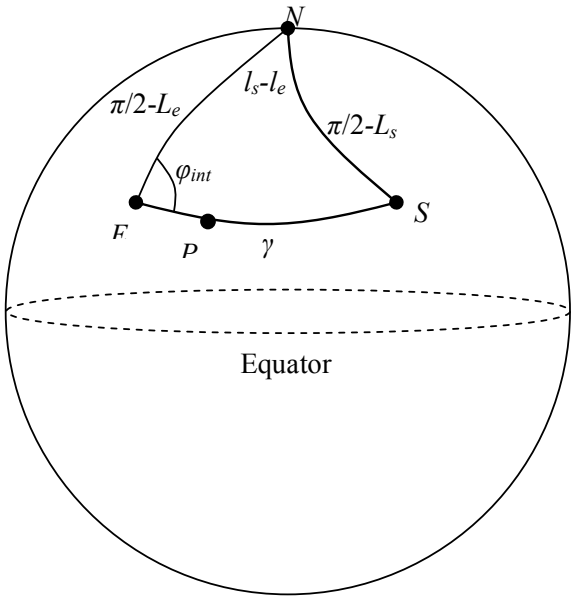

Fig. 1. The spherical triangle defined by the north pole N, the earth station E and the sub-satellite point S. The sublayer point P falls on the geodesic that links the Earth station and the subsatellite point.

where H is the orbital altitude, R_E is the equivalent radius of the Earth after accounting for the effect of the change in refractive index with amplitude (here, we assume a standard atmosphere so the equivalent radius is 4/3 of the actual radius), R_E+H is the distance between the satellite and the centre of the earth and d, the length of the slant path to the satellite, is given by

$$d = \sqrt{R_E^2+(R_E+H)^2-2R_EH\cos\gamma}\,. \quad (4)$$

B. Estimation of the Total and Transverse Velocities

We define the point T_0 as the intersection of the slant path with the middle of the turbulence layer of height h at time t_0 and v as the *total velocity* of the point T_0 across the layer at time t_0. In accordance with the discussion in Section II, we assume that the turbulence layer is generally located between 0.5 and 5 kilometres above the earth's surface.

For the case of a LEO satellite, one can determine v using the geometric construction depicted in Fig. 3(a) and (b) where T_{-1} and T_1 are the locations of the point of intersection at one time interval Δt after and before the current instant, respectively. The magnitude and direction of the total velocity are given by

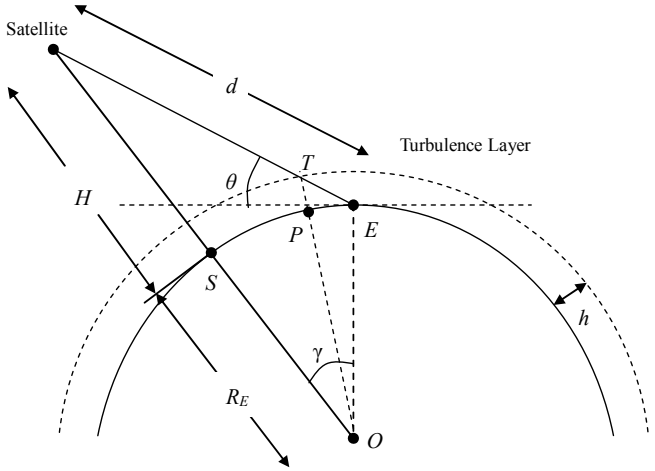

Fig. 2. The geometry of the Earth-space path with respect to the turbulence layer along the great circle that contains the earth station *E*, the sub-satellite point *S*, and the sub-layer point *P*. The remaining symbols are defined in the text.

$$\vec{v} = \frac{\vec{v_0} + \vec{v_1}}{2} = \frac{\overrightarrow{T_{-1}T_0} + \overrightarrow{T_0T_1}}{2}, \tag{5}$$

where $\overrightarrow{T_{-1}T_0} = \overrightarrow{ET_0} - \overrightarrow{ET_{-1}}$, $\overrightarrow{T_0T_1} = \overrightarrow{ET_1} - \overrightarrow{ET_0}$, and *E* is the earth station. As shown in Fig. 3(c), the velocity *v* of T_0 across the top of the turbulence layer at a given instant can be resolved into two components: the along path velocity v_a, which is parallel to the Earth-space path, and the transverse velocity v_t, which is perpendicular to the Earth-space path.

In the case of an overhead pass, the angle α between *v* and v_t depends only upon the elevation angle, and can easily be determined by constructing an appropriate plane triangle. In the general case, however, α is a function of both the elevation and azimuth angles to the satellite. The angle between the vectors $\overrightarrow{T_{-1}T_1}$ and $\overrightarrow{T_0E}$, is the same angle, 90-α, between *v* and v_a, as shown in Fig. 3 (b). Thus, we can show that the angle α is given by

$$\cos\left(\frac{\pi}{2} - \alpha\right) = \frac{\overrightarrow{T_{-1}T_1} \cdot \overrightarrow{T_0E}}{\left|\overrightarrow{T_{-1}T_1}\right|\left|\overrightarrow{T_0E}\right|}. \tag{6}$$

With α known, the transverse velocity can be determined from

$$v_t = v \cdot \cos\alpha. \tag{7}$$

Using a simple geometric construction, one can show that the transverse velocity across a turbulence layer of height *h* will peak at the zenith of an overhead pass. Given that the velocity of the satellite is given by

$$v_{sat} = \sqrt{\frac{GM_E}{R_E + H}}, \tag{8}$$

where $GM_E = 3.986 \times 10^5 \text{ km}^3/\text{s}^2$ is the geocentric gravitational constant, it is then a simple matter to show that the peak transverse velocity at the turbulence layer due to the motion of the satellite is given by

$$v_{t,peak} = \frac{h}{H}\sqrt{\frac{GM_E}{R_E + H}}. \tag{9}$$

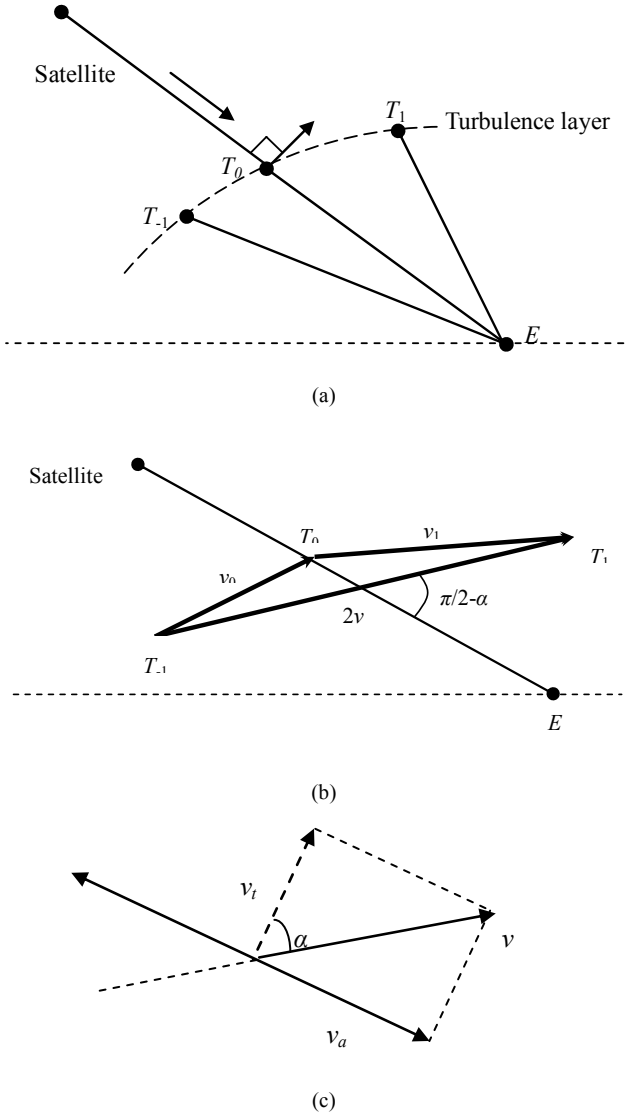

Fig.3. The relationship between the direction to the satellite along the Earth-space path, the total velocity of the Earth-space path across the turbulence layer, and the component of the total velocity that is transverse to the Earth-space path. (a) Determination of total velocity *v* by taking the vector average of v_1 and v_2. (b) Determination of the total velocity, *v*, (c) Determination of transverse velocity v_t.

In practical situations, and particularly in the case of fixed paths such as Earth-GEO links, advection of the turbulence cells by the wind must also be accounted for. We consider this in more detail in Section IV-D.

C. Prediction of the Corner Frequency

The corner frequency f_c of the scintillation power spectrum

can be determined from Tatarskii's theory using [22], which predicts that f_c is proportional to the transverse velocity v_t but inversely proportional to the square root of z, the length of slant path from the earth station to the turbulence layer. The length z is directly proportional to the turbulence layer height h,

$$z = \frac{h}{\sin\theta}. \tag{10}$$

Because the layer height ranges from 0.5 to 5 km and θ ranges from 10 to 90 degrees, z varies over a wide range. Because increasing h also leads to a higher total velocity v and, as a result, higher transverse velocity v_t, the relationship between f_c, h and v_t is complex. In Section IV, we predict and compare the manner in which the corner frequency evolves during a pass for layer heights of 1, 2, 3 and 4 km and satellites in polar orbits with altitudes of 200, 800 and 1500 km. For LEO links, the peak corner frequency occurs at the zenith during an overhead pass, and can be determined by substituting [9] into [22], yielding

$$\begin{aligned} f_{c,\max} &= 1.43\frac{h}{H}\frac{1}{\sqrt{2\pi\lambda h}}\sqrt{\frac{GM_E}{H+R_E}}, \\ &= 1.43\frac{1}{\sqrt{2\pi\lambda}}\sqrt{\frac{GM_E}{R_E+H}}\frac{\sqrt{h}}{H}, \end{aligned} \tag{11}$$

where λ is the wavelength of the carrier.

D. Prediction of the Intensity of Scintillation

In previous work, *e.g.* [16],[26], it has been found that the instantaneous log-amplitude of scintillation on Earth-GEO links generally follows a zero-mean Gaussian distribution with an intensity σ_χ over periods of several minutes where

$$p(X \mid \sigma_\chi) = \frac{1}{\sqrt{2\pi}}\exp\left(-\frac{X^2}{2\sigma_\chi^2}\right), \tag{12}$$

and X is the log-amplitude of the scintillation [16],[26]. Several models have been proposed to predict the mean of the scintillation intensity σ_χ experienced by Earth-GEO links with a specified elevation angle, frequency and antenna parameters [13]-[15]. Rec. ITU-R P.618 [29] suggests a model of the form,

$$\sigma_\chi = \frac{\sigma_{ref} f^{7/12} g(x)}{(\sin\theta)^{1.2}}, \tag{13}$$

where σ_{ref} is the reference (or normalized) scintillation intensity, $g(x)$ is the antenna aperture averaging factor, f is the carrier frequency and θ is the elevation angle.

For a period of one month or longer, ITU-R recommends that the mean value of σ_{ref} be calculated using

$$\overline{\sigma}_{ref} = 3.6\times10^{-3} + 1.03\times10^{-4} N_{wet}, \tag{14}$$

where N_{wet} is the averaged wet term of the radio refractivity which can be determined using the procedure described in Rec. ITU-R P.453 [30]. Over the long term, measurement studies have variously found that σ_χ on Earth-GEO links follows either a Gamma [11],[13] or log-normal distribution [27],[28]. Because σ_{ref} is proportional to σ_χ, we assume that σ_{ref} itself, which is independent of elevation, frequency and antenna effects, is also Gamma or log-normally distributed. If we assume that σ_{ref} follows a Gamma distribution [13],

$$P(\sigma_{ref}) = \frac{\beta}{\Gamma(\alpha)}\cdot\sigma_{ref}^{\alpha-1}\cdot\exp(-\beta\cdot\sigma_{ref}), \tag{15}$$

where

$$\beta = m_\sigma/\sigma_\sigma^2, \quad \alpha = m_\sigma^2/\sigma_\sigma^2, \quad m_\sigma^2 = 10\sigma_\sigma^2, \tag{16}$$

and where m_σ and σ_σ are the mean and standard deviation of σ_{ref}, we can generate values for σ_{ref} that we can apply to successive passes. We emphasize, however, that the suitability of a particular representation for the probability distribution depends strictly upon local climatic factors and our simulation model can use either depending on which representation is deemed to be more appropriate.

For dry scintillation, we calculate the manner in which σ_χ evolves during a LEO satellite pass as follows: (i) determine the mean value m_σ of σ_{ref} from Rec. ITU-R P.618, and calculate σ_σ; (ii) calculate parameters α and β to determine the Gamma distribution; (iii) generate a random value from Gamma distribution as the σ_{ref} for the pass; and (iv) calculate the time-series σ_χ by incorporating the elevation, antenna and frequency effects using equation [13].

For wet scintillation, an alternative model that captures the correlation between σ_χ and rain attenuation is more appropriate. Matricciani [17] proposed a model originated from Tatarskii's theory, and Van de Kamp [18] proposed a statistical model based upon measurements. Based upon ITALSAT measurement, these two methods were made consistent [20]. For the Matricciani model,

$$\begin{aligned} &\sigma_\chi = \sigma_0 \text{ dB}, && \text{if A} \le 1 \text{ dB}, \\ &\sigma_\chi = \sigma_0 A^{5/12} \text{ dB}, && \text{if A} > 1 \text{ dB}, \end{aligned} \tag{17}$$

For the Van de Kamp model,

$$\sigma_\chi = \sigma_0 + 0.02A \text{ dB}, \tag{18}$$

where A is the rain attenuation. Here, σ_0 is the intensity of dry scintillation. Using a wet scintillation model in conjunction with the method for simulating rain fading described in [7], we are able to give a good estimation of time-series σ_χ during a rain event for LEO satellite passes. We present examples in Section V.

IV. Evolution of Scintillation Parameters During Typical LEO Satellite Passes

A. Low Earth Orbits of Particular Significance

Specifying a link to a satellite in a low earth orbit involves many more degrees of freedom than in the geostationary case. The orbital altitude may range from 200 to 2000 km and the inclination angle may range from 0 degrees (equatorial) to 90 degrees (polar) to slightly beyond (sun-synchronous). The orbital altitude affects the minimum and maximum range to the satellite during each pass and the rate at which the satellite moves across the sky, as seen by the earth station. The inclination angle, combined with the latitude of the earth station, affects the probability distribution function of the satellite's elevation angle as seen by the earth station [31]. Here, we have focused our initial efforts to characterize scintillation on Earth-LEO links on satellites in circular polar orbits with altitudes of 200, 800, and 1500 km. While such orbits are broadly representative of those occupied by many Earth observation and scientific satellites, the modeling approach described in the previous section can easily be extended to satellites in orbits with other altitudes, inclinations and ellipticities as required.

B. Evolution of Scintillation Parameters during Typical Passes

The motion of a LEO satellite across the sky causes rapid changes in both the length of the slant path to the turbulence layer and the velocity at which the slant path passes across the turbulence layer. As we showed in Section III, this affects both the intensity of the scintillation process, which generally reaches its maximum value at low elevation angles and/or periods of rain, and the corner frequency of the scintillation process, which generally reaches its maximum value at high elevation angles. Unless otherwise stated, our simulation results refer to dry scintillation and assume a carrier frequency of 20 GHz, an antenna diameter of 1.2 m, an aperture efficiency of 0.56, a turbulence layer height of 1 km, an air temperature of 20 ºC, humidity of 0.6 and a wind speed of 0 m/s.

We begin by selecting the altitude and inclination of the satellite orbit and the latitude and longitude of the earth station. We assume that the earth station has a clear view of the satellite during the entire portion of the pass that is at least ten degrees above the horizon. We use a commercial satellite orbit prediction tool, AGI's Satellite Tool Kit (STK), to predict the azimuth angle, elevation angle and range to the satellite at one-second intervals for many successive passes. This allowed us to determine the corresponding values of the scintillation intensity σ_χ and corner frequency f_c at each instant following the methods in Section III-C and D. In our analysis, we focused on the portions of the satellite pass with an elevation angle greater than 10 degrees.

In Fig. 4, Fig. 5 and Fig. 6, we show how the elevation angle θ, total velocity v, transverse velocity v_t, the corner frequency f_c and the scintillation intensity σ_χ evolve during overhead passes by LEO satellites in 200, 800 and 1500-km polar orbits with a thin layer of turbulence at an altitude of 1 km.

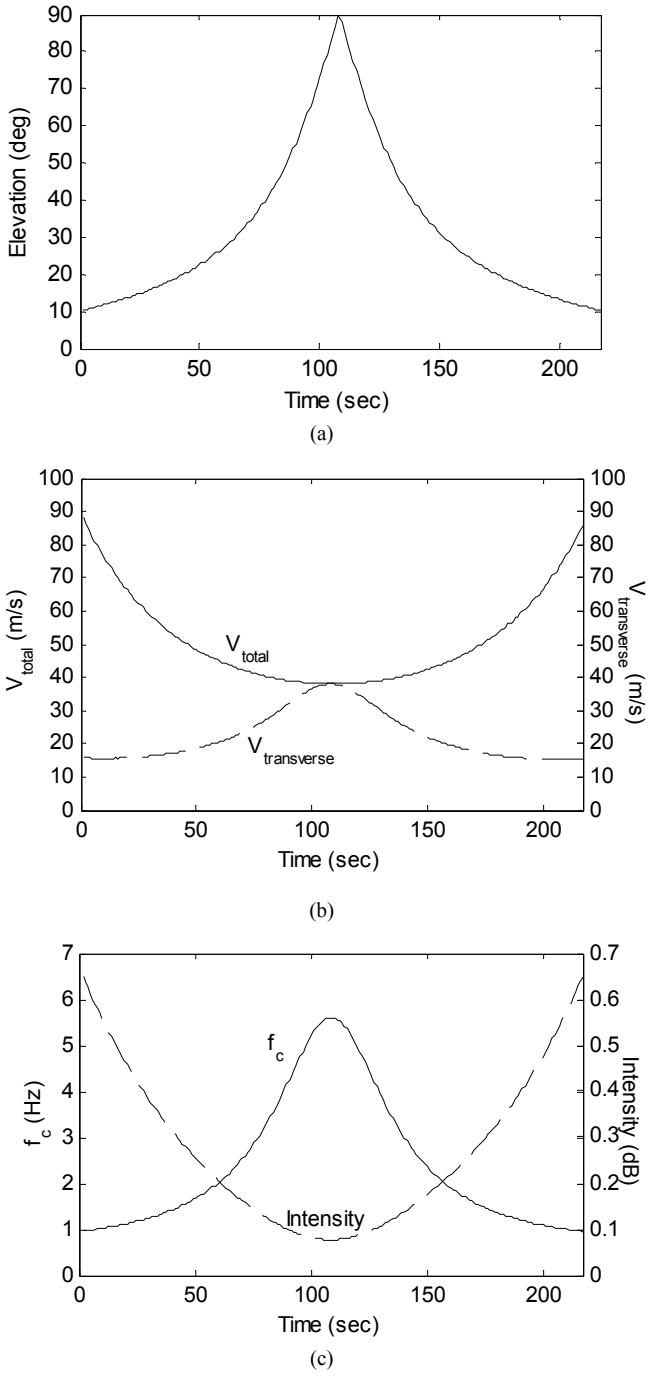

Fig. 4. Typical results for satellite in 200 km polar orbit, with 1 km layer height.

1. As the *elevation angle* increases, it is apparent that: (i) σ_χ decreases with increasing elevation angle, as given in eqn. (14); (ii) the decrease in total velocity v does not imply a corresponding reduction in the transverse velocity v_t, because α, the angle between v and v_t, also decreases; according to eqn. (12), this causes a larger portion of v to contribute to v_t; (iii) the corner frequency f_c reaches a peak value at the highest elevation angle.

The impact of the increased rate of scintillation at high elevation angles is considerably reduced by the sharp reduction in scintillation intensity in such directions.

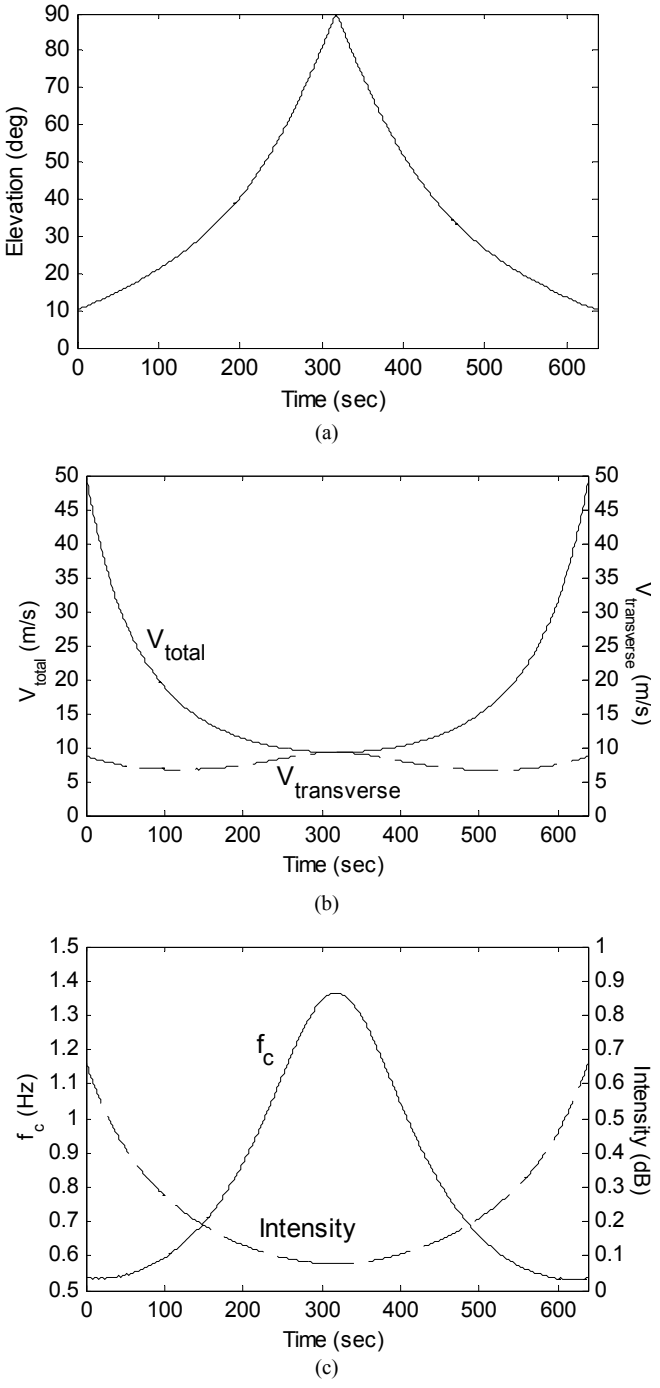

Fig.5. Typical results for satellite in 800 km polar orbit, with 1 km layer height.

2. As the *orbital altitude* increases, it is apparent that: (i) the rate at which the satellite passes through the zenith decreases markedly; (ii) the minimum and maximum values of σ_χ are not affected by changes in the satellite's altitude, while the rate of change decreases because of the slower variation of the elevation angle; (iii) the total velocity v at which the point T crosses the turbulence layer decreases less rapidly as the elevation angle increases, (iv) the transverse velocity v_t (and the corner frequency f_c) experienced during a pass decreases, as suggested by the corresponding reduction of the peak values reported in eqns. (9) and (11). The manner in which σ_χ and f_c evolve with orbital altitude are directly compared in Fig. 7(a) and (b), respectively.

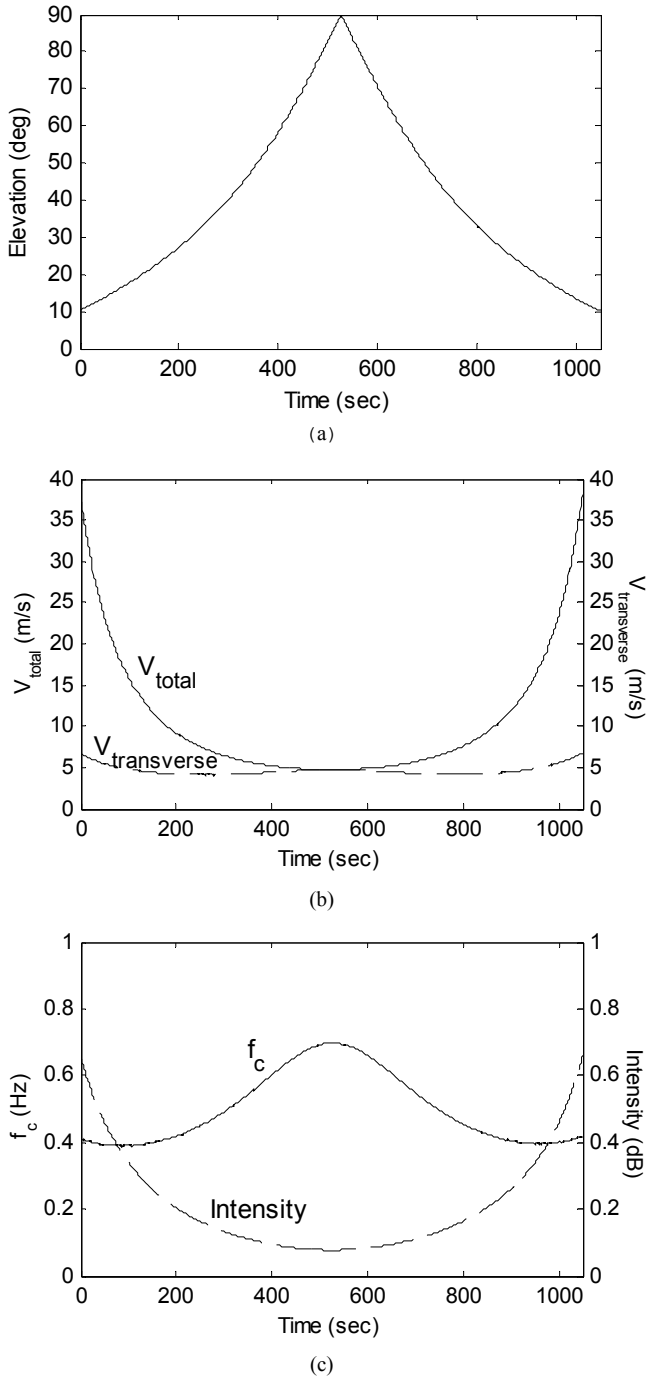

Fig.6. Typical results for satellite in 1500 km polar orbit, with 1 km layer height.

3. As the *height of the turbulence layer* increases, the corner frequency increases substantially, as shown in

Fig. 7(c). Although the increase in h causes both v_t and z to increase, which have contrary effects on corner frequency as discussed in Section III-C, the result shows that the increase in v_t dominates. The peak corner frequencies for 200 km orbit, as shown in Fig. 7(c), correspond closely to those predicted using eqn. (11). For a given satellite altitude, the scintillation intensity is unaffected by the height h of the turbulence layer because the elevation angles are the same.

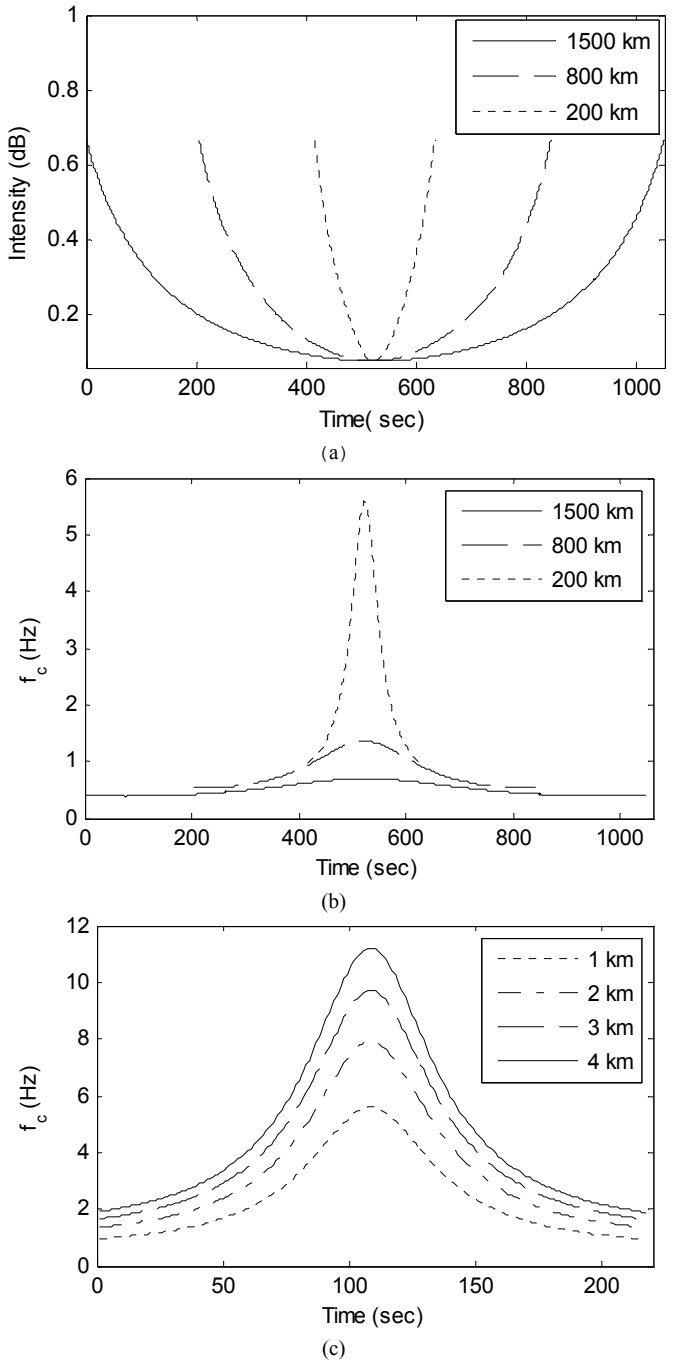

Fig. 7. Evolution of dry scintillation intensity and corner frequency during a pass. (a) Time series dry scintillation intensity, with a 1-km layer height. (b) Time series corner frequency, with 1-km layer height. (c) Time series corner frequencies for satellite in 200 km polar orbits, with turbulence layer at 1, 2, 3 and 4 km altitude.

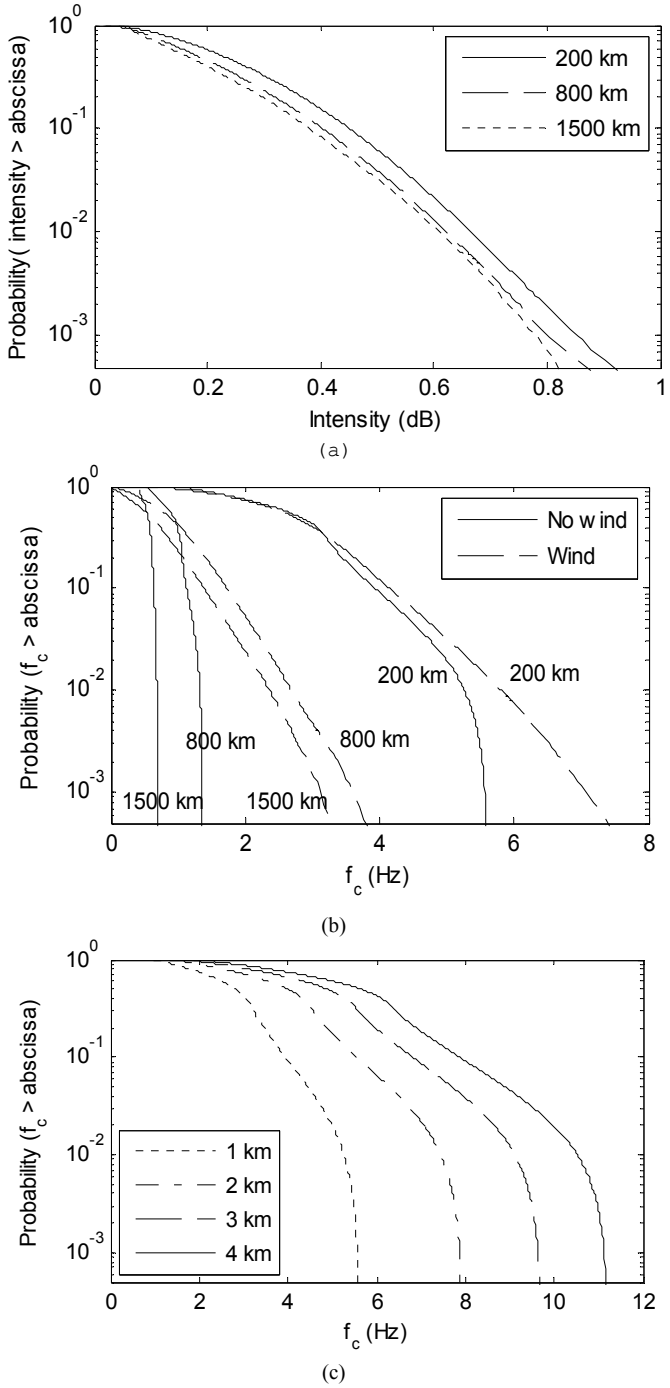

Fig. 8. CCDFs of the dry scintillation intensity and corner frequency. (a) Dry scintillation intensity for different satellite altitudes, with 1-km layer height. (b) Corner frequency for different satellite altitudes and a 1-km layer height, with and without wind. (c) Corner frequency for different layer heights for a satellite in a 200-km polar orbit.

C. Statistics of Scintillation Parameters Over Multiple Passes

In Fig. 8(a), we present the CCDF of the scintillation intensity taken over hundreds of passes. We have included for the tendency for the intensity of the scintillation process to follow its own Gamma distribution over the long term, as described in Section II-E. As the satellite altitude increases the shape of the

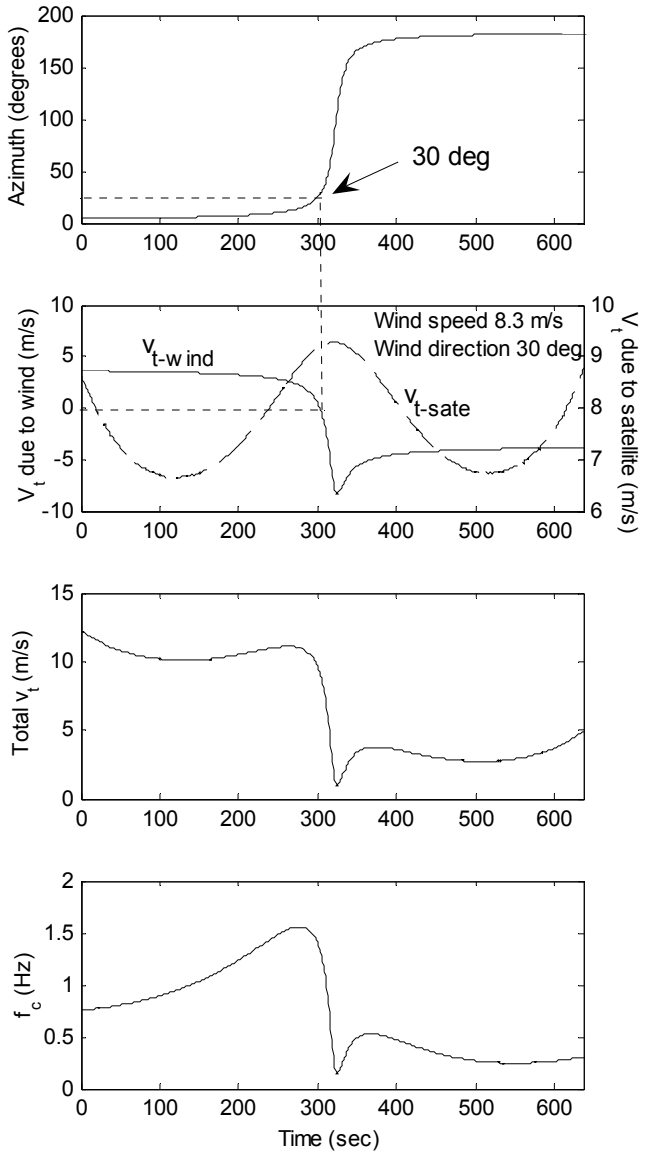

Fig. 9. Evolution of the corner frequency of scintillation during an overhead pass by a satellite in an 800-km orbit with an 8.3 m/s wind blowing at 30 degrees: (a) Evolution of the azimuth angle during the pass. (b) Contributions of wind and satellite motion to the transverse velocity during the pass. (c) Evolution of the total transverse velocit during the pass. (d) Evolution of the corner frequency during the pass.

CCDF of σ_χ evolves as shown in Fig. 8(a) because the fraction of time that the satellite spends at higher elevation angles also increases.

In Fig. 8(b) we present the CCDF of the corner frequency taken over hundreds of passes with the turbulence layer at a height of 1 km and satellite altitudes of 200, 800 and 1500 km, both for cases with and without wind. In practice, the turbulence layer will likely take on a range of values over multiple passes. Using a fixed value allows one to more easily interpret the effect of satellite altitude. It is apparent that: (i) at higher satellite altitudes (800 and 1500 km), the CCDF of corner frequency drops off very suddenly which indicates that only a very narrow range of values of f_c are experienced by the link, (ii) at lower altitudes (200 km), the range of corner frequencies experienced on the link increases but the probability of encountering a peak value is fairly rare. In Fig. 8(c), we fix the satellite altitude and allow the layer height to vary. In particular, we show the CCDFs of the corner frequency for the turbulence layer at heights of 1, 2, 3 and 4 km and the satellite at an altitude of 200 km. The result shows that higher corner frequencies are reached at higher layer altitude, and wider range of f_c are experienced by the link.

D. Wind Effects on Corner Frequency

As discussed in Section III-C, advection of turbulence cells past the Earth-space path by the wind contributes a random component to the transverse velocity that must be accounted for when predicting the corner frequency f_c of the scintillation process. In practice, the distribution of wind velocity is both location and time dependent. For the purposes of demonstration, we have followed previous work and accepted an assumption that the wind speed in mid-latitude temperate climates tends to follow a log-normal distribution over the long term with a median value of 8.33 m/s and a standard deviation of $log_e 2$ [25]. Further, we assume that wind direction is uncorrelated with wind speed and follows a uniform distribution. Because a LEO satellite pass is only several minutes in length, we assume that the wind velocity is constant for the duration. As the direction of the azimuth angle changes during the pass, the wind's contribution to the transverse velocity, v_{t_wind} , also changes.

A typical result for a satellite in an 800-km orbit is shown in Fig. 9. The evolution of the azimuth angle during the pass is shown in Fig. 9(a). The contributions of wind and satellite motion to the transverse velocity as the pass evolves are shown in Fig. 9(b). In this case, the transverse velocity v_{t_wind} decreases to zero when the azimuth angle points into the wind. The manner in which the total transverse velocity and corner frequency are distorted as the pass evolves is shown in Fig. 9(c) and (d). In Fig. 8(b), the CCDFs of the corner frequency over the long term for satellites in 200, 800 and 1500-km orbits are presented with and without account taken for wind. It is apparent that advection of turbulence cells by the wind may cause relatively large changes in f_c, that cannot be ignored.

V. Generation of Scintillation Time Series

When simulating fade mitigation techniques or assessing scintillation suppression methods, it is usually necessary to provide time series data that mimic actual scintillation, *i.e.,* have the same first and second-order statistics. One method for generating scintillation time series that are representative of those observed on Earth-GEO links involves passing additive white Gaussian noise (AWGN) through a filter with a suitable low pass response then adjusting the scintillation intensity to the correct value [20]. Two cases are of particular interest: (i) in the absence of precipitation, *i.e.,* dry scintillation, the scintillation intensity is typically determined using the model contained in Rec. ITU-R P.618 while the distribution of the

scintillation intensity over the long term may be described by a Gamma distribution, as described in [13], or a log-normal distribution, as described in [26]. (ii) In the presence of precipitation, *i.e.,* wet scintillation, the scintillation intensity depends upon the instantaneous depth of rain fading and can be calculated using either of the techniques described in [17] and [18], as described in Sec. III-D. An alternative approach to simulating wet scintillation involves interpolating between the samples in a rain attenuation time series subject to the assumption that scintillation can be modeled as fractional Brownian motion [32].

A dynamic model of tropospheric scintillation on Earth-GEO links is described in [21]. Because both the corner frequency and the scintillation intensity evolve rapidly during a pass, Earth-LEO links introduce additional complications when simulating scintillation time series by low pass filtering white Gaussian. Filters with time-varying parameters are relatively simple to implement but care must be taken to avoid transient behavior when the filter parameters are updated [33],[34]. Our time-varying scintillation time-series generator is based upon an AWGN generator followed by a fourth order low pass filter whose coefficients are updated every sample. Following [20], we used the Yule-Walker equations to estimate the low pass filter coefficients required to realize a scintillation process with the Tatarskii spectrum (see the Appendix). Because the scintillation power spectrum rolls off at -80/3 dB^2/Hz, the frequency response of the corresponding spectral shaping filter must be designed to roll off at -40/3 dB/Hz.

Simulation of a scintillation time series proceeds as follows. One applies AWGN signal to the spectral shaping filter, and then, for every sample, one updates the filter coefficient according to the instantaneous corner frequency that one predicts using the geometric model presented in Section III-C. Finally, one scales the signal that appears at the filter output in order to obtain the desired scintillation intensity. Although our time series generator updates the spectral shaping filter every sample, it may be desirable in some cases to reduce the computational load by updating the filter once per frame. We leave this possibility and determination of the ideal frame length for future study.

In Fig. 10, we show the manner in which dry scintillation might evolve during an overhead pass by a LEO satellite in a 1500-km polar orbit, and on an Earth-GEO link with a fixed elevation angle of 30 degrees. It is apparent that: (i) at low elevation angles (at the start and the end of the pass), more intense scintillation is observed, and (ii) at high elevation angles, the variation of the signal is relatively small. In Fig. 11, we show a typical result for wet scintillation during an overhead pass by a LEO satellite in a 1500-km polar orbit, with a maximum elevation angle of 22 degrees. The underlying rain fade event was predicted using the method described in [7]. The large deep fade during the descending portion of the pass is due an intense rain cell in the immediate vicinity of the ground terminal. Substantial increases in scintillation intensity that are predicted by our model can be seen: (i) at the start and end of the pass, where they are a result of low elevation angle effects and (ii) near t = 500 seconds of elapsed time, where they are the result of a sudden increase in rain attenuation. Both the underlying rain fade event and the manner in which

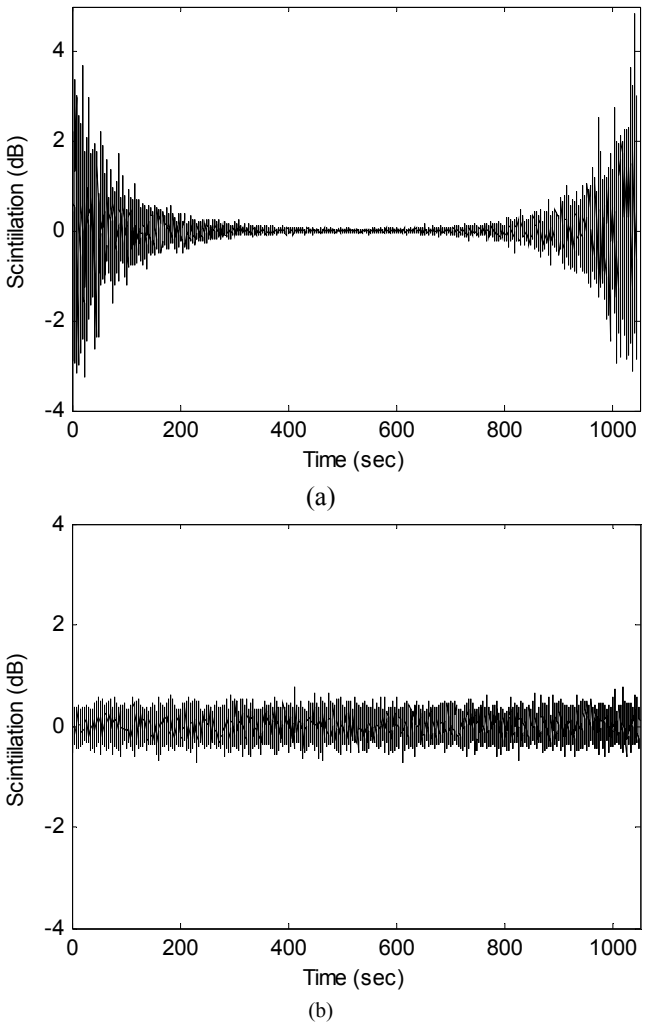

Fig. 10. Evolution of dry scintillation intensity over time for typical links to satellites in both LEO and GEO. (a) Dry scintillation intensity during a pass by a satellite in a 1500-km polar orbit. (b) Dry scintillation intensity to a satellite in GEO at an elevation angle of 30 degree over the same duration as in (a).

scintillation evolves are superficially similar to anecdotal results obtained using FEDSAT [6]. Not enough information concerning the FEDSAT data is available to permit more detailed comparison.

Here, for lack of more detailed information concerning the spatial or height distribution of turbulence, we have assumed that the refractive index structure constant C_n^2, hence the value of σ_{ref}, and the turbulence height are constant over the entire field. In practice, it seems likely that the structure constant and turbulence height will change as the path passes from horizon and intersects different parts of the sky. Resolution of this issue will likely have to await general availability of actual measurement data from Earth-LEO Ka-band links or results obtained by other means.

VI. Conclusions

We have used Tatarskii's theory in conjunction with a geometric model of propagation through a uniform turbulence layer of broad extent during a LEO satellite pass to show how the amplitude and rate of the scintillation process will evolve as

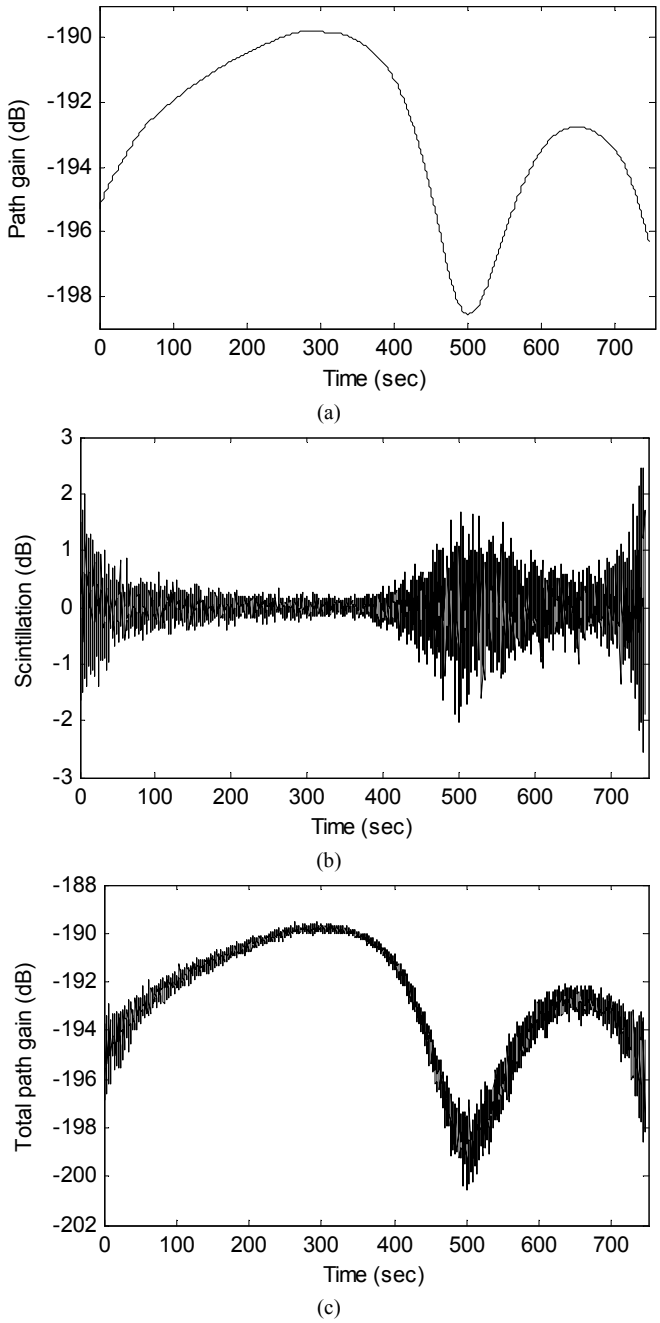

Fig. 11. Accounting for wet scintillation during a pass by a satellite in a 1500-km polar orbit. (a) Evolution of path gain during the pass with account taken for range, atmospheric gases, cloud and fog, and rain fading only. (b) Evolution of wet scintillation during the pass. (c) Evolution of total path gain, including wet scintillation, during the pass.

a function of the orbital altitude and height of the turbulence layer. While the amplitude of the scintillation process is only determined by the elevation angle to the satellite, the maximum corner frequency increases markedly as the orbital altitude decreases. The time-varying nature of the corresponding scintillation power spectrum makes it necessary to use time-varying filters when simulating scintillation on LEO links and introduces an extra level of complexity compared to simulation of scintillation on GEO links.

While our simulations have revealed the general manner in which the scintillation process will likely evolve during a LEO satellite pass and offer physical insight, the accuracy of our results is limited by our need to assume that the horizontal structure and height of the turbulence layer are constant over each pass and our use of representative rather than site-specific wind velocity statistics. Verification of the assumptions that underlie our model and precise determination of the relevant model parameters must await the general availability of measurement data collected during many LEO satellite passes. Research concerning the large-scale structure of turbulence is being pursued by various groups and the outcomes of that work will greatly benefit simulations using the methods presented here. Until more extensive measurement data is available, simulation studies of the type presented here are likely the best option for developing immediately useful insights concerning the nature of scintillation during LEO satellite passes. In the future, models of this type will also provide a reference against which the measurement data can be assessed and interpreted.

APPENDIX – TATARSKII'S THEORY OF SCINTILLATION

Most models of scintillation on Earth-space links, including ours, are based upon the theory proposed by Tatarskii [10] based upon earlier work by Kolmogorov. Here we briefly review the theory and consider its assumptions before applying it to scintillation on Earth-LEO Ka-band links. If one can assume that the atmospheric turbulence is locally homogeneous, isotropic and frozen [35],[36], Kolmogorov's theory of turbulence can be used to predict the variance of the scintillation amplitude. Kolmogorov's theory characterizes turbulence eddies on two scales, the outer turbulence scale L_0 and the inner turbulence scale l_0 where, in the troposphere, L_0 is between 10 and 100 metres, corresponding to the instability of the medium, and l_0 is of the order of 1 mm, which is related to the fluid viscocity. When the eddy size s falls within the inertial subrange between L_0 and l_0, the turbulence is isotropic, and the spectrum density is expressed by

$$\Phi_n(\kappa) = 0.033 C_n^2 \kappa^{-11/3} \quad \text{for} \quad \frac{2\pi}{L_0} < \kappa < \frac{2\pi}{l_0}, \tag{19}$$

where $\kappa = 2\pi/s$ and C_n^2 is the structure constant of the refractive index.

Subject to the assumptions [16] that: (i) $l_0 << \sqrt{\lambda L} << L_0$, (ii) the incident wave is a plane wave and (iii) scintillation is weak[1], *i.e.,* $\sigma_\chi^2 << 1$, Tatarskii [10] showed that the variance of the amplitude of a plane wave traveling through the turbulence layer is

$$\begin{aligned} \sigma_\chi^2 &= 0.307 C_n^2 k^{7/6} L^{11/6} \ \text{Np}^2 \\ &= 23.17 C_n^2 k^{7/6} L^{11/6} \ \text{dB}^2, \end{aligned} \tag{20}$$

where λ is the wavelength, k is the wave number and L is the distance through the turbulence layer. Tatarskii also showed

[1] Some previous work has shown that assumption (iii) is valid for up to 0.2~0.5 dB^2, or 0.8 dB^2 of σ_χ^2.

that the scintillation spectrum can be expressed by

$$W_\chi^0(f) = \frac{64.17}{f_0} C_n^2 k^{7/6} z^{11/6} \quad (dB^2/Hz) \quad f \ll f_c \ , \qquad (21)$$
$$W_\chi^\infty(f) = \frac{165.15}{f_0} C_n^2 k^{7/6} z^{11/6} \left(\frac{f_0}{f}\right)^{-8/3} \quad (dB^2/Hz) \quad f \gg f_c \ ,$$

where z is the slant path distance to the turbulence layer and f_0 is the Fresnel frequency given by

$$f_0 = \frac{v_t}{\sqrt{2\pi\lambda z}}, \qquad (22)$$

and v_t is the transverse velocity. The corner frequency f_c is defined as the intersection between the two asymptotes and is equal to $1.43 f_0$.

For Ka-band (20/30 GHz) frequencies, the wavelength λ falls between 0.01 and 0.015 metres. When the layer height h falls within the range 0.5 to 5 km, z falls between 5.8 and 28.8 km at the lowest elevation angle that we shall consider, $\theta = 10°$. Over this range, $\sqrt{\lambda z}$ takes on values between 9 and 20 metres which satisfies the first of the three assumptions given earlier. The extreme range between the satellite and the earth station ensure that the incident wave is plane while experimental results collected over the years confirms that the amplitude of the scintillations observed on Earth-space links at Ka-band is generally low. Thus, Tatarskii's theory applies.

ACKNOWLEDGMENT

We thank Cesar Amaya and David V. Rogers of the Communications Research Centre, Ottawa for helpful discussions and comments.

REFERENCES

[1] D. V. Rogers, L. J. Ippolito, Jr. and F. Davarian, "System requirements for Ka-band earth-satellite propagation data," *Proc. IEEE,* vol. 85, no. 6, pp. 810–820, June 1997.

[2] P. J. Brown, "Ka- band Payloads Proliferate as Business Model Fall in Place," *Via Satellite Magazine*, pp. 16-23, May 2006.

[3] J. V. Evans, "Proposed U.S. global satellite systems operating at Ka-band," *Proc. IEEE AeroConf.*, 21-28 Mar. 1998, pp. 525-537.

[4] F. Lansing, L. Lemmerman, A. Walton and G. Bothwell, "Needs for communications and onboard processing in the vision era," in *Proc. IEEE IGARSS'02*, 24-28 Jun. 2002, pp. 375-377.

[5] G. Giffin, K. Magnussen, M. Wlodyka, L. Duffield, B. Poller and J. Bravman, "CASCADE: A Ka-band smallsat system providing global movement of extremely large data files," in *Proc. IEEE MILCOM'05*, 17-20 Oct. 2005, pp. 550-556.

[6] T. Kostulski and S. Reisenfeld, "Ka band propagation experiments on the Australian low-Earth orbit microsatellite 'FedSat'," in *Proc. 6th Australian Communications Theory Workshop*, 2005, pp. 102-106.

[7] W. Liu and D. G. Michelson, "Fade slope analysis of Ka-band Earth-LEO satellite links using a synthetic rain field model," *IEEE Trans. Veh. Technol.*, in press.

[8] J. Feil, L. J. Ippolito, Jr., H. Helmken, C. E. Mayer, S. Horan and R. E. Henning, "Fade slope analysis for Alaska, Florida and New Mexico ACTS propagation data at 20 and 27.5 GHz," *Proc. IEEE,* vol. 85, no. 6, pp. 925-935, June 1997.

[9] M. M. J. L. van de Kamp, "Statistical analysis of rain fade slope," *IEEE Trans. Antennas Propag.,* vol. 51, no. 8, pp. 1750-1759, Aug. 2003.

[10] V. I. Tatarskii, *Wave Propagation in a Turbulent Medium*. New York: McGraw-Hill, 1961.

[11] C. E. Mayer, B. E. Jaeger, R. K. Crane and X. Wang, "Ka-band scintillation: Measurements and model predictions," *Proc. IEEE*, vol. 85, no. 6, pp. 936-945, June 1997.

[12] H. Vasseur and D. Vanhoenacker, "Characterisation of tropospheric turbulent layers from radiosonde data," *Elec. Lett.,* vol. 34, no. 4, pp. 318-319, 19 Feb. 1998.

[13] Y. Karasawa, M. Yamada and J. E. Allnutt, "A new prediction method for tropospheric scintillation on Earth-space paths," *IEEE Trans. Antennas Propag.*, vol. 36, no. 11, pp. 1608-1614, Nov. 1988.

[14] I. E. Otung, "Prediction of tropospheric amplitude scintillation on a satellite link," *IEEE Trans. Antennas Propag.*, vol. 44, no. 12, pp. 1600-1608, Dec. 1996.

[15] M. M. J. L. van de Kamp, J. K. Tervonen, E. T. Salonen and J. P. V. P. Baptista, "Improved models for long-term prediction of tropospheric scintillation on slant path," *IEEE Trans. Antennas Propag.*, vol. 47, no. 2, pp. 249-260, Feb. 1999.

[16] H. Vasseur, "Prediction of tropospheric scintillation on satellite links from radiosonde data," *IEEE Trans. Antennas Propag.*, vol. 47, no. 2, pp. 293-301, Feb. 1999.

[17] E. Matricciani, M. Mauri and C. Riva, "Relationship between scintillation and rain attenuation at 19.77 GHz," *Radio Sci.*, vol. 31, no. 2, pp. 273-279, March-April 1996.

[18] M. M. J. Van de Kamp, "Tropospheric scintillation measurements and modeling in Finland," in *Proc. IEE ICAP'97,* Edinburgh, U.K., 14-17 Apr. 1997, pp. 141-144.

[19] A. Savvaris, C. N. Kassianides and I. E. Otung, "Observed effects of cloud and wind on the intensity and spectrum of scintillation," *IEEE Trans. Antennas Propag.*, vol. 52, no. 6, pp. 1492-1498, Jun. 2004.

[20] J. Lemorton, L. Castanet, F. Lacoste, M. van de Kamp, C. Riva, E. Matricciani and U-C Fiebeg, "Development of propagation models for telecommunications satellite systems", ESA/ESTEC Contract No. 16865/03/NEL/EC, Final report, Jul. 2004.

[21] C. N. Kassianides and I. E. Otung, "Dynamic model of tropospheric scintillation on earth-space paths", IEE Proc. Microw. Antennas Propag., vol. 150, no. 2, pp. 97–104, 2003.

[22] P. Yu, I. A. Glover, P. A. Watson, O. T. Davies, S. Ventouras, C. Wrench, "Review and comparison of tropospheric scintillation prediction models for satellite communications," *Int. J. Satell. Commun. Networking*, vol. 24, no. 4, pp. 283-302, 2006.

[23] S. A. Borgsmiller, "Effects of atmospheric scintillation in Ka-band satellite communications," *PhD thesis*, Georgia Institute of Technology, Atlanta, GA, 1998.

[24] E. Masciadri, R. Avila and L. J. Sánchez, "First evidence of the finite horizontal extent of the optical turbulence layers. Implications for the new adaptive optics techniques," *Astron. Astrophys.*, vol. 382, no. 1, pp. 378-388, 2002.

[25] E. Matricciani, "Physical-mathematical model of the dynamics of rain attenuation based on rain rate time series and a two-layer vertical structure of precipitation," *Radio Sci.*, vol. 31, no. 2, pp. 281-295, 1996.

[26] I. E. Otung and B. G. Evans, "Short term distribution of amplitude scintillation on a satellite link," *Electron. Lett.*, vol. 31, no. 16, pp. 1328-1329, Aug. 1995.

[27] T. J. Moulsley and E. Vilar, "Experimental and theoretical statistics of microwave amplitude scintillations on satellite down-links," *IEEE Trans. Antennas. Propag.*, vol. AP-30, no. 6, pp. 1099-1106, Nov. 1982.

[28] G. Ortgies, "Probability density function of amplitude scintillations," *Electron. Lett.*, vol. 21, no. 4, pp. 141-142, Feb. 1985.

[29] "Propagation data and prediction methods required for the design of Earth-space telecommunication systems," Rec. ITU-R P.618-9, ITU, Geneva, 2007.

[30] "The radio refractive index: Its formula and refractivity data," Rec. ITU-R P.453-9, ITU, Geneva, 2003.

[31] S. Y. Li and C. H. Liu, "An analytical model to predict the probability density function of elevation angles for LEO satellite systems," *IEEE Commun. Lett.,* vol. 6, no. 4, pp. 138-140, April 2002.

[32] N. Celandroni and F. Potorti, "Modeling Ka-band scintillation as a fractal process," *IEEE J. Sel. Areas Commun.*, vol. 17, no. 2, pp. 164-172, Feb. 1999.

[33] R. Rabenstein, "Minimization of transient signals in recursive time-varying digital filters," *Circ. Syst. Signal Process.,* vol. 7, no. 3, pp. 345-359, 1988.

[34] V. Välimäki and T. I. Laakso, "Suppression of transients in variable recursive digital filters with a novel and efficient cancellation method," *IEEE Trans. Signal Process.*, vol. 46, no. 12, pp. 3408-3414, Dec. 1998.
[35] G. I. Taylor, "The spectrum of turbulence," *Proc. R. Soc. A.* vol. 164, no. 919, pp. 476-490, Feb. 1938.
[36] G. E. Willis and J. W. Deardorff, "On the use of Taylor's translation hypothesis for diffusion in the mixed layer," *Quart. J. R. Met. Soc,* vol. 102, pp. 817-822, 1976.

Weiwen Liu received the B.Eng. degree in electrical engineering from Harbin Institute of Technology, Harbin, China, in 2006. She recently completed the M.A.Sc. degree with the Department of Electrical and Computer Engineering, University of British Columbia, Vancouver, BC, Canada.

Her main research interests include propaga- tion and channel modeling for Ka-band satellite communications.

David G. Michelson (S'80–M'89–SM'99) received the B.A.Sc., M.A.Sc., and Ph.D. degrees from the University of British Columbia (UBC), Vancouver, BC, Canada, all in electrical engineering.

From 1996-2001, he served as a member of a joint AT&T Wireless Services (Redmond, WA) and AT&T Labs – Research (Red Bank, NJ) team concerned with development of propagation and channel models for next generation and fixed wireless systems. The results of this work formed the basis for the propagation and channel models later adopted by the IEEE 802.16 Working Group on Broadband Fixed Wireless Access Standards. From 2001-2002, he helped to oversee deployment of one of the world's largest campus wireless LANs at the University of British Columbia while also serving as an adjunct professor in the Department of Electrical and Computer Engineering. Since 2003, Prof. Michelson has led the Radio Science Lab at UBC where his current research interests include propagation and channel modeling for fixed wireless, UWB and satellite communications.

Professor Michelson is a registered professional engineer. He serves as Chair of the IEEE VT-S Technical Committee on Propagation and Channel Modeling and as an Associate Editor for Mobile Channels for IEEE Vehicular Technology Magazine. In 2002, he served as a guest editor for a pair of special issues of IEEE Journal on Selected Areas in Communications concerning propagation and channel modeling. From 2001-2007, he served as an Associate Editor for IEEE Transactions on Vehicular Technology. From 1999-2007, he chaired the IEEE Vancouver Section's Joint Communications Chapter. Under his leadership, the Chapter received Outstanding Achievement Awards from the IEEE Communications Society in 2002 and 2005, and the Chapter of the Year Award from IEEE Vehicular Technology in 2006. He received the E.F. Glass Award from IEEE Canada in 2009 and currently serves as Chair of Vancouver Section.